Journal of Sustainable Cement-Based Materials

ISSN: (Print) (Online) Journal homepage: www.tandfonline.com/journals/tscm20

Enhancing the properties of carbonation cured gamma dicalcium silicates (γ-C_2S) using biomimetic molecules

Muhammad Intesarul Haque, Ishrat Baki Borno & Warda Ashraf

To cite this article: Muhammad Intesarul Haque, Ishrat Baki Borno & Warda Ashraf (2024) Enhancing the properties of carbonation cured gamma dicalcium silicates (γ-C_2S) using biomimetic molecules, Journal of Sustainable Cement-Based Materials, 13:5, 690-705, DOI: 10.1080/21650373.2023.2300964

To link to this article: https://doi.org/10.1080/21650373.2023.2300964

Journal of Sustainable Cement-Based Materials, 2024
Vol. 13, No. 5, 690–705, http://dx.doi.org/10.1080/21650373.2023.2300964

Enhancing the properties of carbonation cured gamma dicalcium silicates (γ-C_2S) using biomimetic molecules

Muhammad Intesarul Haque[#], Ishrat Baki Borno and Warda Ashraf*

Department of Civil Engineering, The University of Texas at Arlington, Arlington, Texas, USA

This study investigates the effectiveness of three different organic molecules to enhance the properties of carbonated gamma dicalcium silicate (γ-C_2S) based cementitious system. These molecules are addressed as biomimetic molecules due to their ability to mimic the biomineralization process. Low dosages (2.5% and 5%) of L-aspartic acid (LAsp), L-glutamic acid (LGlu) and polyacrylic acid (PAA) were incorporated to the γ-C_2S paste. The effects of these molecules on the microstructure, CO_2 sequestration capacity and strengths of the CO_2-activated γ-C_2S pastes were monitored. To understand the effectiveness of molecules at different temperature, the compressive and flexural strengths of γ-C_2S pastes carbonated at 25 °C and 50 °C were evaluated. It was observed that all the molecules enhanced the strength of the composites by altering the $CaCO_3$ formation and subsequent densification of the matrix. However, the effectiveness of the molecules varies depending on the temperature. Specifically, LGlu and LAsp were found to be the most and the least, respectively, effective molecule at high temperature (50 °C) carbonation curing condition; whereas, PAA remained nearly equally effective at both temperatures.

Keywords: Carbonation; gamma dicalcium silicates; biomimetic molecules; microstructure; nano-mechanical performance; mechanical strength

1. Introduction

In recent times, there has been a growing call for the development of alternative and eco-friendly binder systems, and this demand has been prompted by the significant carbon footprint associated with ordinary portland cement (OPC) [1–6]. A recent inclusion among these alternative cementitious systems is the carbonation-activated low-lime calcium silicate binder [7,8]. Notably, these low-lime phases, which have been historically disregarded in OPC due to their hydraulic limitations, exhibit a remarkable enhancement in reactivity when exposed to CO_2 [9–11]. Capitalizing on the potential of these calcium silicates provides an exceptional chance to tackle the carbon footprint of cement production. By reducing temperature requirements and clinker production, these materials offer promising solutions for more sustainable cement manufacturing [7,8, 12,13].

Among the calcium silicates, dicalcium silicate (C_2S) can potentially lower the energy needed for cement manufacturing by 0.29 to 0.42 GJ/ton of clinker when employed as the principal cement constituent (for example, belite-based binders) [13–16]. Even though Portland cement largely comprises β-C_2S, in recent studies, γ-C_2S has received attention for several reasons. The γ-C_2S crystal stands out as the most stable among the five polymorphs of dicalcium silicates, exhibiting minimal hydraulic activity at room temperature [17,18]. While γ-C_2S is less active than β-C_2S [14, 19], its unique ability to generate fine powders during production, aptly termed the 'dusting' effect, remarkably diminishes grinding energy requirements, setting it apart from traditional C_3S [14, 19]. γ-C_2S has been identified as an eco-friendly construction material with exceptional CO_2-absorption abilities [20]. Carbonation activated γ-C_2S blended cementitious composites have shown potential to produce carbon negative concrete [21–23]. Moreover, research indicates that wollastonite (CS) and rankinite (C_3S_2) behave similarly as that of γ-C_2S when exposed to carbonation curing owing to the traditional non-hydraulic behavior [7, 9,10]. Therefore, knowledge of γ-C_2S's carbonation reactivity can give direction for activation of low-carbon calcium silicate-based cementitious materials.

Most of the previous studies on carbonated γ-C_2S samples were performed after preparing the specimens under molding pressure and high temperature curing [24–27]. These applied pressure and elevated temperature enabled the non-hydraulic γ-C_2S samples to achieve a very high strength when cured under 99% CO_2 concentration. However, it is also understandable that the application of such pressure and temperature during the production process increases the overall carbon footprint of the composites. Therefore, any potential pathway to enhance the mechanical performance of γ-C_2S samples carbonated at room temperature can further reduce the energy consumption and the associated carbon footprint of such composites.

A potential pathway to enhance the mechanical performance of Ca-rich carbonated cementitious composites, is to control the characteristics of $CaCO_3$ – the primary binding phase in these composites. The mechanical

*Corresponding author. Email: warda.ashraf@uta.edu
[#]Structural Engineer II, HNT B Corporation, Baltimore, Maryland, USA.
Supplemental data for this article can be accessed online at https://doi.org/10.1080/21650373.2023.2300964.

performance of carbonated cement composites shows considerable variation due to the presence of different $CaCO_3$ polymorphs [7, 10]. Among the different $CaCO_3$ polymorphs, amorphous calcium carbonate (ACC) first forms inside capillary pores, and later, it converts to metastable phases – vaterite or aragonite due to nucleation, growth, and transition which eventually ends up forming the stable calcite [28,29]. This metastable calcium carbonate polymorphs' formation is responsible for improved mechanical strengths [30,31]. Hence, controlling these polymorphs' formation is important to achieve better carbonated cementitious properties, but it is challenging to control these polymorph formations which depend on factors like humidity, temperature, CO_2 concentrations, water contents etc. [31–34]. Apart from fine-tuning these parameters, a variety of organic molecules can be used to control the polymorph formation in carbonated cementitious composites. Researchers utilized amino acids and other biomolecules - ovalbumin, lysozyme, and bovine serum albumin (BSA) to modify $CaCO_3$ polymorphs [30, 35–38]. Ovalbumin and lysozyme had been used to modify the $CaCO_3$ morphology [36]. BSA was incorporated into $CaCO_3$ which was synthesized using the gas-diffused method and, the formation of $CaCO_3$ with hierarchical structures were observed [37]. Several amino acids have been successfully incorporated to improve the performances of carbonated wollastonite composites by Khan et al. [30]. Later, the effects of proteins with different molecular structures were investigated in carbonated wollastonite composites by Baffoe and Ghahremaninezhad [33]. In addition to amino acids, polyacrylic acid can be a reasonable alternative since it also showed the potential to control the crystallization of $CaCO_3$ [39]. These biomimetic molecules develop organic-inorganic composites in cementitious matrixes which play a key role in obtaining remarkable mechanical properties [30, 33]. However, the effectiveness of such organic molecules on the carbonation behavior of γ-C_2S have not been explored yet.

Considering this knowledge gap, interest was triggered to explore and enhance the properties of carbonation activated γ-C_2S based cementitious materials with the addition of biomimetic molecules. Therefore, for this study, two amino acids - L-aspartic acid (LAsp) and L-glutamic acid (LGlu) were chosen along with polyacrylic acid (PAA) to observe their ability to enhance the nano and micro-structural properties of carbonated γ-C_2S composites. The hypothesis is these biomimetic molecules can alter the $CaCO_3$ polymorphs formation which will eventually enhance the micro and nano-mechanical performance of the carbonated γ-C_2S composites. For this, micro to nano structural analyses were performed on carbonated γ-C_2S composites to verify the hypothesis. The effects of the biomimetic molecules on compressive and flexural strengths of γ-C_2S pastes carbonated at 25 °C and 50 °C were evaluated to understand the effectiveness of this approach at different temperatures. In this study, the primary aim was to investigate the potential of biomimetic molecules in low calcium cementitious composites, aiming for a greener and more sustainable cement-concrete construction industry.

2. Materials and methods

2.1. Raw materials

Various techniques exist for the synthesis of pure calcium silicate phases [40–42]. Most of these methods involve employing the technique of sintering a stoichiometric mixture of lime and silica. In this study, $CaCO_3$ (>99% purity) and fumed silica (>99% purity) were used to synthesize γ-C_2S. As mentioned earlier, L-aspartic acid ($C_4H_7NO_4$; MW 133.10 and high purity grade), L-glutamic acid ($C_5H_9NO_4$; MW 147.13 and high purity grade) and polyacrylic acid (50 wt% solution in water, approximate MW 5000) were used as the biomimetic molecules. All these raw materials and biomimetic molecules were purchased through VWR.

2.2. Sample preparation

A uniform mixture of $CaCO_3$ and fumed silica was prepared with a molar ratio of 2:1. To facilitate the mixing process, water-to-binder (w/b) ratio was maintained at 0.65. The resulting paste mixture was then placed in a high-temperature furnace resistant crucible. The crucible was heated at a rate of 4.5 °C per min and then hold at 1400 °C for 4 h. The relatively high sintering temperature for producing γ-C_2S was selected based on the literature to achieve high degree of conversion rate [25]. Afterward, it was allowed to cool down slowly within the furnace to room temperature, ensuring the stabilization of γ-C_2S.

The sintered products were then ground and sieved through a mesh #200 (74 μm). To optimize the chemical reaction between available lime and silica, the resulting powder was subjected to two additional firing cycles. X-ray diffraction (XRD) analysis was performed after each sintering cycle to verify the absence of any free lime contents.

Furthermore, thermogravimetric analysis (TGA) was utilized to monitor the free lime content of the synthesized γ-C_2S, ensuring it remained below 3%. These steps were undertaken to synthesize and verify the desired properties of γ-C_2S for potential applications.

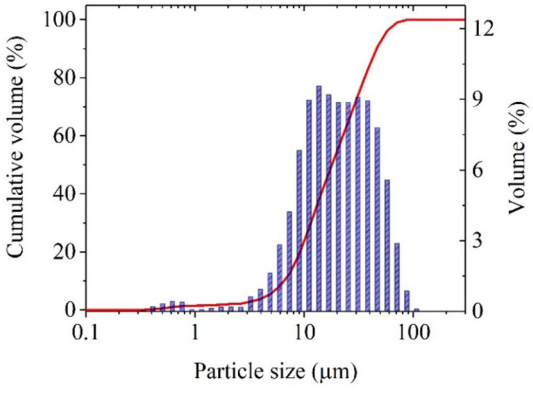

Figure 1. Particle size distribution of the synthesized γ-C_2S.

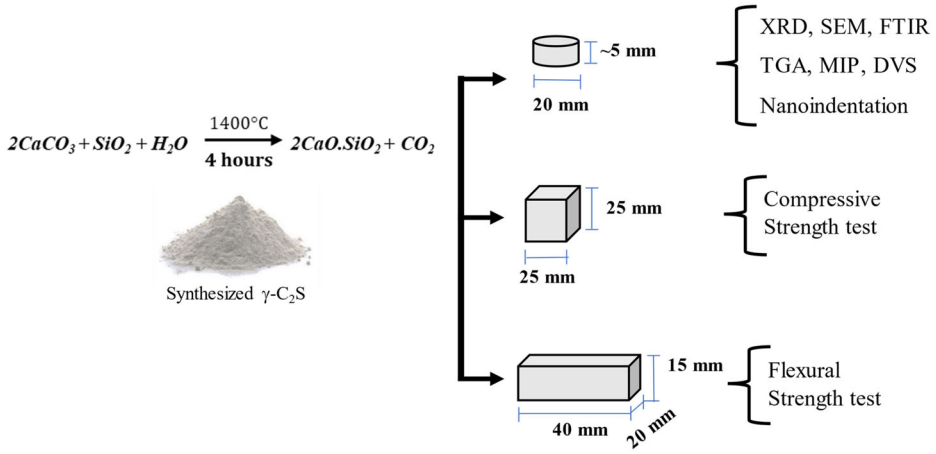

Figure 2. Schematic diagram of the sample preparation.

The particle size distribution of the synthesized γ-C_2S is shown in Figure 1 which was determined using a commercially available laser particle size analyzer.

Two types of samples were prepared for carbonation curing: (i) thin disc from paste samples (~5 mm thick and 20 mm Dia) and (ii) compacted paste cube and beam samples. The first type of samples was used to monitor the $CaCO_3$ polymorph formation and evolution along with nanomechanical properties during the carbonation period. The second category was prepared for mechanical strength and pore size distribution analysis. For preparing the paste samples, dry biomimetic molecules were first mixed with water at 2.5% and 5% concentration (by weight percentage of γ-C_2S). The control batch contained no biomimetic molecules. γ-C_2S powder was then mixed using a high shear mixer (at 350 rpm for 2 min). The water to binder (w/b) ratio was maintained as 0.40 throughout the experimental process. Then the paste samples were used to prepare beam and cubes samples (the cube-shaped samples measured 25 mm × 25 mm × 25 mm, while the beam-shaped samples were 40 mm × 20 mm × 15 mm) using silicon molds. The samples were compacted by hand tamping and no external pressure was applied. The samples with the molds were then placed inside a commercially available carbonation chamber setting the relative humidity at 80% and CO_2 concentration at 20%. The samples were demolded after 24 h and placed back in the carbonation chamber. Separate set of samples were carbonated at 25 °C and 50 °C to evaluate the effect of temperatures. Figure 2 shows the schematic diagram of the sample preparation of each experiment.

2.3. Test methods

2.3.1 X-ray diffraction (XRD)

Samples of carbonated paste were gathered after 7 days and subsequently ground to prepare them for X-ray diffraction (XRD) analysis. These powdered samples were loaded into a Bruker D500 spectrometer, where a Cu Kα radiation (40 kV, 30 mA) was employed. The diffraction patterns were then recorded in the 2θ range of 10° to 60° with a step size of 0.03 (2θ) per second.

Phase identification through X-ray diffraction (XRD) was carried out using commercially available software known as 'Match! Phase Analysis using Powder Diffraction'. The PDF card numbers used for reference were as follows: PDF #96-900-0967 for calcite, PDF #96-901-3802 for aragonite, PDF #96-150-8972 for vaterite, and PDF #96-154-6026 for γ-C_2S.

2.3.2. Scanning electron microscopy (SEM)

The microstructures of the carbonated γ-C_2S pastes were analyzed using the Hitachi S4800 II FE-SEM. Operating in high-vacuum mode, the instrument employed a 30-kV accelerated voltage and maintained a working distance of approximately 11 mm. Before capturing the SEM images, the cement paste sample was coated with Gold (Au)-Platinum (Pt). The analysis utilized the powder form of the paste samples.

2.3.3. Fourier transform infrared spectroscopy (FTIR)

Fourier-Transformed Infrared (FTIR) spectra of the ground paste sample were obtained using the Attenuated Total Reflection (ATR) mode, employing a resolution of 4 cm^{-1} and conducting 32 scans for each sample. The signal to noise ratio was maintained below 3:1. The FTIR test was performed on carbonated samples collected after 7 days.

2.3.4. Thermogravimetric analysis (TGA)

The TGA experiment of the paste sample was conducted using a commercially available instrument (TA instrument, TGA 550). The paste samples, which had been stored in a vacuum desiccator, were used for this test. To prepare the samples, they were ground with a mortar pestle until a fine powder was obtained. Around 25–30 mg of the powdered sample, passing through a #200 sieve, was loaded into a platinum pan. The pan was subjected to an isothermal condition at 25 °C for 5 min before gradually increasing the chamber temperature to 980 °C at a rate of 15 °C per minute. To ensure an inert environment, nitrogen gas was purged during the process.

To validate the consistency of carbonation across samples, the TGA test was initially performed with three replicate samples. The results showed a deviation of less than 2% by weight of total carbonated samples, indicating good reproducibility. Consequently, for the remaining batches, TGA was performed with only one sample due to the low level of deviation.

2.3.5. Mercury intrusion porosimeter (MIP)

The Micrometrics Instrument Corporation AutoPore IV 9500 V2.03.01 was utilized to conduct Mercury intrusion porosimeter (MIP) experiments on cementitious composites. This technique is employed to determine the structure of meso-porous (pore radius $2 \sim 50$ nm) and macro-porous (> 50 nm) materials. The MIP test was carried out on three sets of samples: the control batch, and paste samples with 2.5% and 5% dosages, all subjected to carbonation curing for 7 days. The sample size was standardized to $15 \times 15 \times 15$ mm.

In the MIP experiment, mercury was used with a surface tension of 0.485 N/m and an average contact angle of 130° with the pore wall. The maximum pressure applied was 413 MPa, allowing the examination of pores with a diameter as small as 3.02 nm. This analysis helps in characterizing the pore structures of the cementitious composites in different dosage conditions after the carbonation curing period.

2.3.6. Dynamic vapor sorption test (DVS)

To obtain the moisture desorption isotherm of carbonated paste samples, the commercially available DVS equipment (TA instrument, Q5000) was employed. Prior to testing, the samples were immersed in DI water for 6 h to ensure complete saturation. About 4–5 mg of the saturated sample was loaded into a quartz pan.

The desorption isotherm was obtained by first equilibrating the sample at 97.5% relative humidity (RH) for 5760s. Subsequently, the RH was gradually reduced in steps of 5–10% to achieve desorption. At each RH level, mass equilibrium was considered reached when the sample's mass fluctuation remained below 0.001% for 15 min. The entire experiment was conducted at a constant temperature of 23 °C, and nitrogen gas was consistently purged during the process to maintain a stable environment.

DVS is the favored method for assessing meso and gel pore structures in cementitious phases, as opposed to mercury intrusion porosimetry (MIP) [43]. When compared to water sorption, the nitrogen sorption technique significantly underestimates the surface area of cementitious matrix. This article utilized the BET method to determine the surface area (S_{BET}) of carbonated composites. [44] and pore size distribution was determined based on the BJH model [45]. The calculation of the BET and BJH methods can be found elsewhere [46,47].

2.3.7. Nanoindentation

For the nanoindentation tests, a Hysitron Triboindenter UB1 system (Hysitron Inc., Minneapolis, USA) equipped with a Berkovich diamond indenter probe was utilized. To ensure accurate measurements, the tip area function was calibrated using multiple indents with varying contact depths on a standard fused quartz sample. The surface roughness was evaluated using the Berkovich tip, and in all instances, it was found to be below 80 nm over an area of $60\,\mu m \times 60\,\mu m$. This level of surface quality was deemed suitable for conducting nanoindentation tests.

For grid nanoindentation, 7 days carbonated samples were specifically chosen. The load function adopted a three-segment approach: (i) a 5-s loading process from zero to maximum load, (ii) a 5-s hold at the maximum load, and (iii) a 5-s unloading from maximum to zero load. To accurately determine the mechanical properties of individual microscopic phases, it was essential to ensure that the depth of indentations remained considerably smaller than the characteristic size of each microscopic phase (indentation depth $\ll$ characteristic size of each microscopic phase) [48]. Therefore, for this study using the SNI technique, a maximum force of 2000 μN was selected. As a result, the average indentation depth within a $30\,\mu m \times 30\,\mu m$ area ranged from approximately 100–300 nm.

2.3.8. Compressive and flexural strength testing

To measure the compressive strength, a Gilson compressive strength testing machine was employed, applying a loading rate of 450 N/s. On the other hand, the flexural strength, determined through the 3-point bending test, was measured using a laboratory-made micro-mechanical tester with a displacement rate of 1 mm/min.

After 7 days of carbonation curing, the compressive and flexural strength of paste samples were evaluated. The cube-shaped samples measured 25 mm × 25 mm × 25 mm, while the beam-shaped samples were 40 mm × 20 mm × 15 mm.

To observe the effects of high temperature curing, another set of samples were prepared for both compressive and flexural strength testing and kept inside the carbonation chamber at 50 °C for 7 days (maintaining the same other parameters; 20% CO_2 concentration, 80% RH).

3. Results

3.1. Effects on the carbonation extent and CO_2 sequestration

Figure 3 illustrates the thermogravimetric analysis (TGA and DTG) graphs of 7 days carbonated samples. The observed mass losses in the temperature range of 300–800 °C for the 7 days cured paste samples can be attributed to the decomposition of $CaCO_3$ phases [14]. The occurrence of multiple DTG peaks within this temperature range is associated with the decomposition of various polymorphs of $CaCO_3$ [30, 46, 49]. The TGA results were

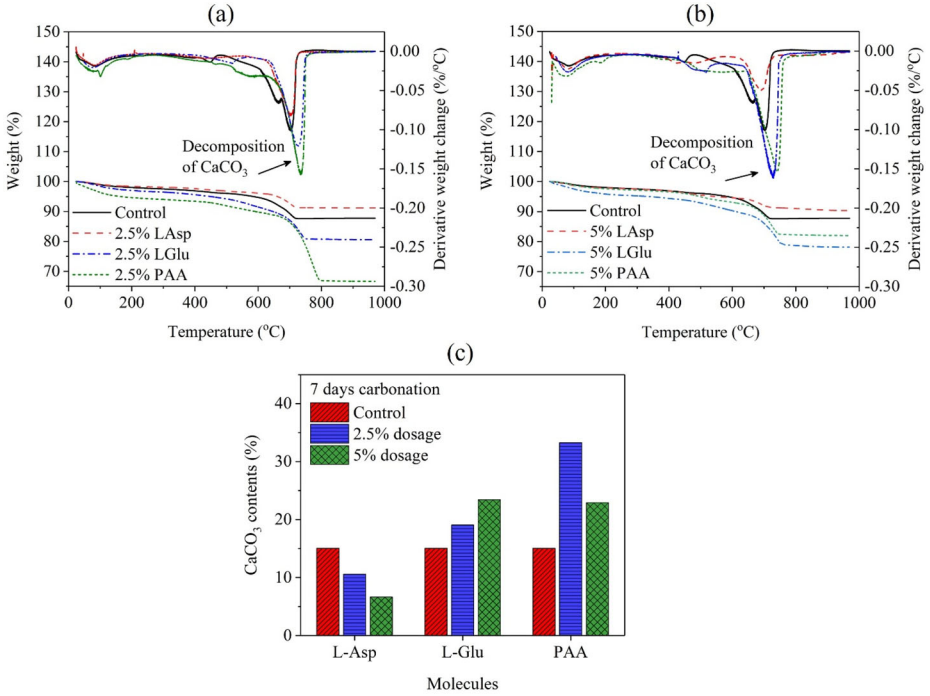

Figure 3. Thermogravimetric analysis of 7 days carbonated γ-C_2S paste samples; (a) 2.5% batches, (b) 5% batches, (c) comparison of $CaCO_3$ contents formation among the batches.

utilized to determine the total $CaCO_3$ content that underwent decomposition within the temperature range of 400–800 °C (Figure 3(c)). Noteworthy, this temperature range was selected instead of a lower range (i.e. from 300 °C) to avoid the contribution from the evaporation of chemically-bound water present in ACC which evaporates at around 200 to 350 °C as per the literature [30].

It was observed that with the increase in the dosage of LAsp, the $CaCO_3$ contents decreased. This observation matches with previous findings on the role of LAsp in carbonated wollastonite composites [30]. For LGlu batches, the observation was opposite to that of LAsp. Increasing the dosage of LGlu increased carbonate formation, and therefore, the degree of carbonation. In PAA modified batches, 2.5% batch showed the highest amount of $CaCO_3$ contents. Accordingly, while the addition of LAsp reduced the CO_2 sequestration capacity of γ-C_2S, the other two molecules increased the sequestration capacity. The CO_2 stored in the carbonated composite increased by nearly 46% due to the addition of 5% LGlu and by around 110% due to the addition of 2.5% PAA, indicating the effectiveness of these molecules to enhance carbon sequestration capacity of the composites.

3.2. *Effects of molecules on the $CaCO_3$ polymorphs: observations from XRD, FTIR and SEM*

Figure 4 shows the XRD patterns of the 7-days carbonated γ-C_2S paste samples. The XRD pattern of the synthesized γ-C_2S matched with previously published literature [14, 50]. Both the γ-C_2S and the calcite peak were identified at a very close range ($\sim 29^\circ$ 2θ). From Figure 4(a), it is observed that 2.5% PAA modified γ-C_2S batch showed the highest calcite peak ($\sim 29^\circ$ 2θ). Nevertheless, 2.5% PAA modified batch showed the formation of aragonite and vaterite as well. The other 2.5% biomimetic molecule modified batches showed comparatively less prominent calcite peak formation. However, all the 2.5% batches showed metastable $CaCO_3$ polymorphs (vaterite and aragonite) formation.

From Figure 4(b), it can be observed that calcite peak (around 29.6°) got reduced for the 5% LAsp and PAA containing batches, which corroborates the findings from TGA. With the increase of the LGlu dosage, the γ-C_2S peak intensity was observed to decrease. Other metastable $CaCO_3$ polymorphs peak was also observed in the 5% batches, but those were not prominent. Aragonite formation was also observed in the control batch.

Apart from the XRD patterns, the formation of carbonate polymorphs in the modified γ-C_2S samples was also investigated using FTIR spectra (Figure 5). The added molecules did not significantly alter the CSH or silica gel structure of the paste samples and therefore, the FTIR spectra corresponding to the silica gel structure (800 to 1200 cm^{-1}) range are not discussed here and provided as supplementary data (Supplementary Figure S1). FTIR peaks due to the asymmetric stretching (ν_3) and in-plane bending vibration (ν_4) of CO_3^{2-}, located at around 1450 cm^{-1} and 712 cm^{-1}, respectively, were used for this study. The peak due to the in-plane bending vibration (ν_4) of CO_3^{2-} (after background removal) was used to distinguish the carbonate polymorphs. Noteworthy, the peak at around 1450 cm^{-1} (corresponding to asymmetric stretching (ν_3) of CO_3^{2-}) is often used to identify the presence of vaterite/ACC in the carbonated composite in literature [30]. However, the peak at 1450 cm^{-1} is generally overlapped by the presence of all carbonate polymorphs. The peaks in the 690 cm^{-1} to 755 cm^{-1} range shows clearly distinguishable peaks for different carbonate polymorphs [51]. They are at 700 cm^{-1} for aragonite, at 712 cm^{-1} for calcite and at 746 cm^{-1} for vaterite (all these bands are due to the in-plane bending vibration

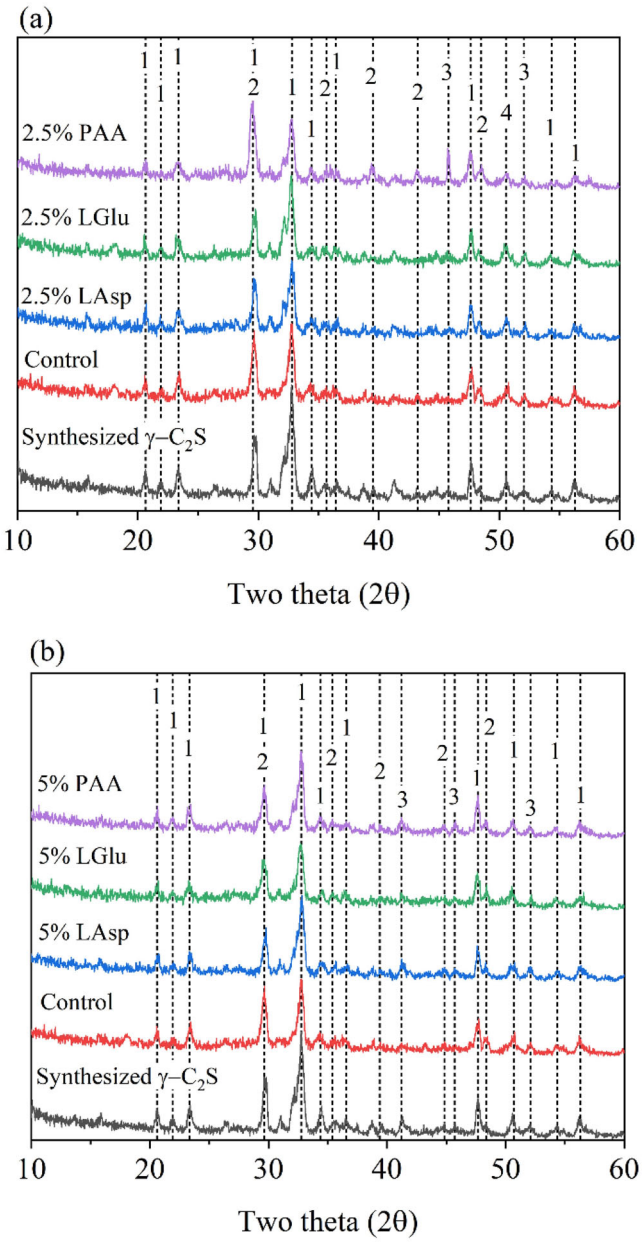

Figure 4. X-ray diffraction pattern of the γ-C2S paste, (a) 2.5% batch and (b) 5% batch. (1: γ-C2S, 2: Calcite, 3: Aragonite, and 4: Vaterite).

(ν_4)) [52–57]. Important to note, ACC formation does not show any peak in this wavenumber range, and therefore, allowing clear distinction between vaterite and ACC.

From the observation, both the 2.5% and 5% PAA and LGlu modified γ-C_2S carbonated paste samples showed calcite peak at 712 cm^{-1}. A small aragonite peak was identified in the control and 2.5% PAA containing batches. The 2.5% LAsp batch showed low intensity of calcite and vaterite peaks. However, at 5% LAsp dosage, the ν_4 peak associated with the crystalline calcium carbonates (i.e. calcite, vaterite, and aragonite) disappeared or significantly reduced. On the other hand, the FTIR peak at around 1400 cm^{-1} confirms the formation of carbonates in this 5% LAsp sample. Therefore, combining the observations from both asymmetric stretching (ν_3) and in-plane bending vibration (ν_4) of CO_3^{2-}, it can be suggested that primarily ACC formed in this 5% LAsp sample.

The morphology of the γ-C_2S paste samples prepared with and without different biomimetic molecules was evaluated using SEM. The control sample exhibited calcite crystals with sharp rhombohedral edges (Figure 6(a)). The 2.5% LAsp (Figure 6(b)) and 2.5% PAA (Figure 6(d)) contained spherical ACC and vaterite phases. In 2.5% LAsp sample, the ACC spheres were larger in diameter (200 nm, 20-point average with a standard deviation of 38 nm) and agglomerated together, whereas in 2.5% PAA, the crystal sizes were smaller (60 nm, 20-point average with a standard deviation of 17 nm), and spheres were agglomerated. It was interesting to note that both 2.5% and 5% LGlu (Figures 6(c) and 7(c), respectively) samples contained vaterite with different crystal sizes and shapes. A relatively larger crystal of calcite with rounded edges compared to the control sample was observed in 5% dosages of LAsp and PAA (Figure 7(b) and (d), respectively). In the 5% LAsp sample, there were no

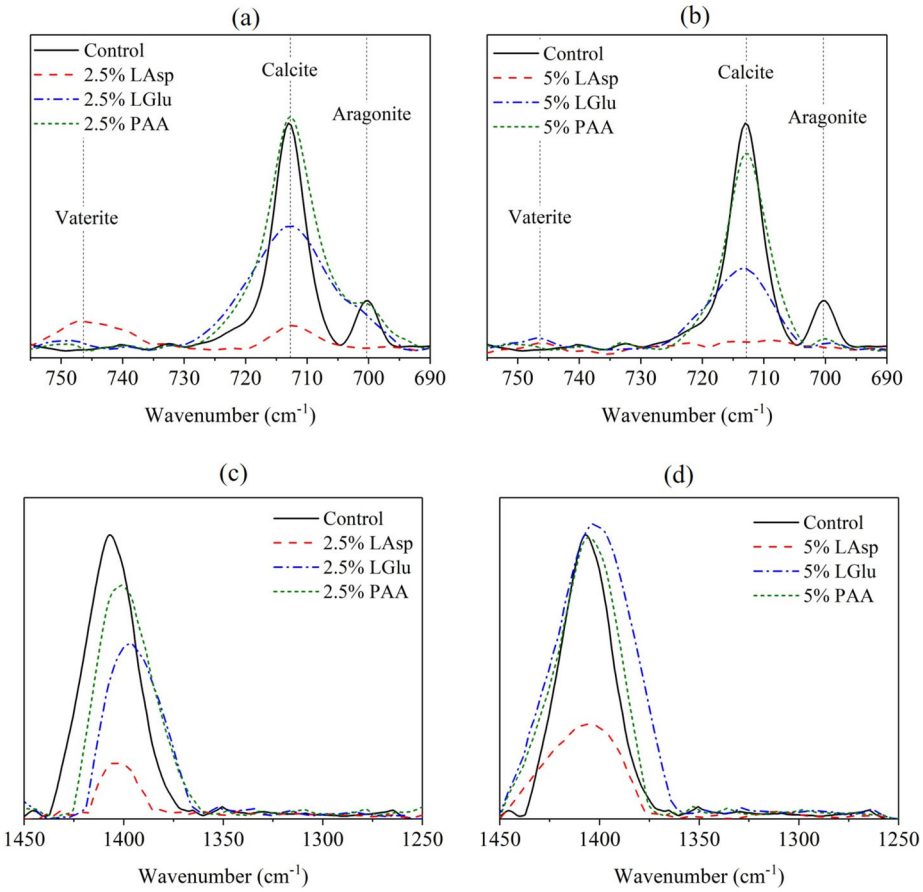

Figure 5. FTIR spectra of 7 days carbonated biomimetic molecules modified γ-C_2S paste samples; (a) 2.5% batch at 700–750 cm^{-1}; (b) 5% batch at 700–750 cm^{-1}; (c) 2.5% batch at 1400 cm^{-1}; (d) 5% batch at 1400 cm^{-1}.

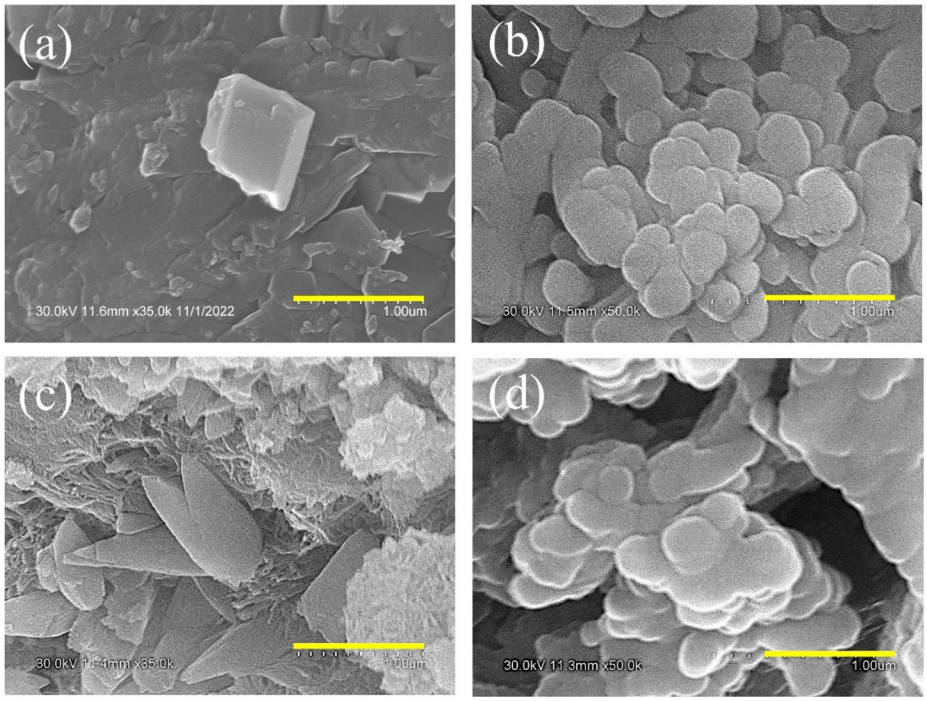

Figure 6. Morphology of the calcium carbonate polymorphs in (a) control, (b) 2.5% LAsp, (c) 2.5% LGlu, and (d) 2.5% PAA samples. The scale bar represents 1 μm.

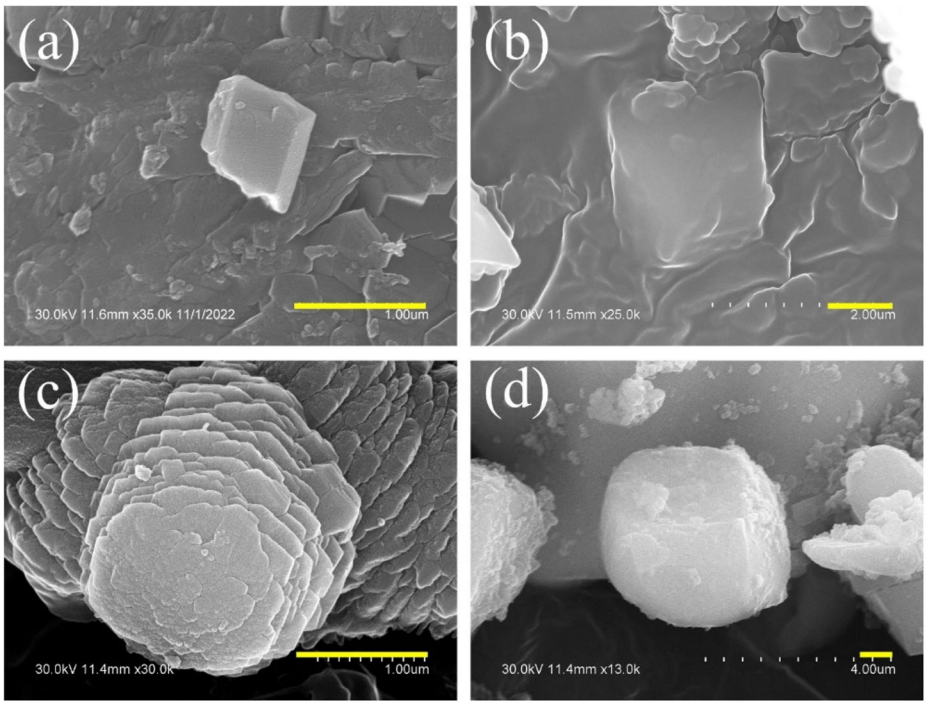

Figure 7. Morphology of the calcium carbonate polymorphs in (a) control, (b) 5% LAsp, (c) 5% LGlu, and (d) 5% PAA samples. The scale bar represents 1 μm.

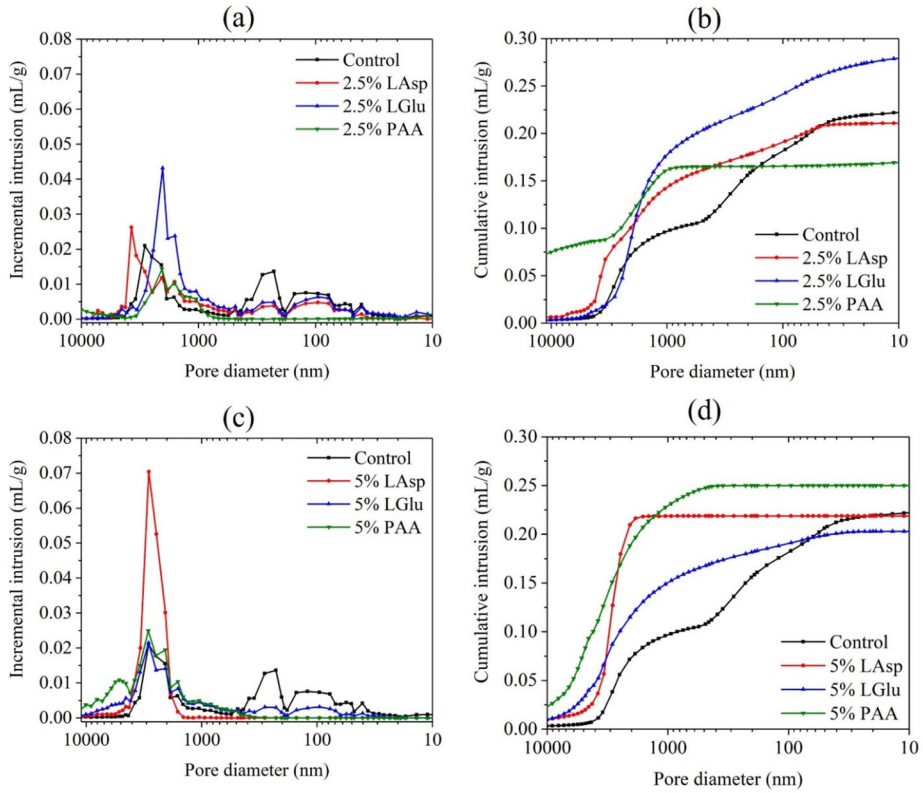

Figure 8. Effects of biomimetic molecules on pore size distribution of 7 days carbonated γ-C_2S paste samples.

individual crystals of calcium carbonate observed throughout the sample. However, it appeared that the carbonate phases were covered with extra deposition, as presented in Figure 7(b). Vaterite was observed in both 5% LGlu and 5% PAA batches.

3.3. Effects on the micro and nanoscale pore size distribution

Pore size distributions of the 7 days carbonated γ-C_2S paste samples as obtained using MIP are presented in Figure 8 and the quantitative comparison due to the

addition of the biomimetic molecules on the pore structure is given in Table 1.

Compared to the control batch, the addition of 2.5% LGlu increased the total porosity by 19% and reduced the critical pore diameter (i.e. pore diameter corresponding to the highest intensity of pores). The addition of 2.5% PAA and 2.5% LAsp reduced the total porosity by 23% and 5%, respectively compared to the control batch. Therefore, the addition of these molecules enabled the formation of a denser microstructure. The addition of 5% LAsp showed nearly the same total porosity as compared to the control batch, however with a significant increase in the large porosity. Such formation of large porosity is due to the reduced degree of carbonation (as observed from TGA) after the addition of 5% LAsp. The 5% LGlu containing batch showed a reduced porosity compared to the control batch. The addition of 5% PAA resulted in an increase of the total porosity without altering the critical pore size compared to the control batch. The pore size distribution as obtained from MIP matches well with the observations from TGA. Specifically, at 2.5% dosage, PAA showed the highest degree of carbonation and the lowest total porosity. In the case of 5% dosage, LGlu showed the highest carbonate formation and the lowest total porosity.

Table 1. Effects on the pore structure (7 days carbonated samples) obtained by MIP.

Batch	Porosity (%)	Total pore area (m^2/g)
Control	34.95	7.34
2.5% LAsp	33.15	2.61
2.5% LGlu	41.74	6.24
2.5% PAA	26.91	2.54
5% LAsp	35.13	0.29
5% LGlu	31.53	1.647
5% PAA	37.12	0.41

DVS is commonly regarded as a more appropriate method for characterizing and analyzing meso-scale and gel pore structures in cementitious materials that contain CSH or Ca-modified silica gels. In this aspect, it proves to be more efficient compared to MIP or nitrogen sorption procedures [47]. The nano pore size distributions of the carbonated γ-C_2S composites with and without the biomimetic molecules are shown in Figure 9. From these graphs, three major peak locations were noticed. They are at 5 Å, 8 Å and 11.5 Å. The peak location at 11.5 Å is the corresponding peak due to the porosity of the interlayers in calcium silicate hydrates (CSH) or Ca-modified silica gel structures [52]. After the addition of the biomimetic molecules, no peak shift occurred which indicates the biomimetic molecules do not affect the silicate structure. However, addition of these biomimetic molecules resulted in reduced interlayer porosity indicating lower amount of CSH/Ca-modified silica gel formation. The specific surface area is correlated with the quantity of water-accessible fine pores [47]. The specific surface area (S_{BET}) of completely hydrated cement paste typically falls within the range of 100–200 m^2/g [58]. Carbonated calcium silicates are known to have lower S_{BET} compared to hydrated cement paste [46]. As observed from Figure 9(c) and (d),

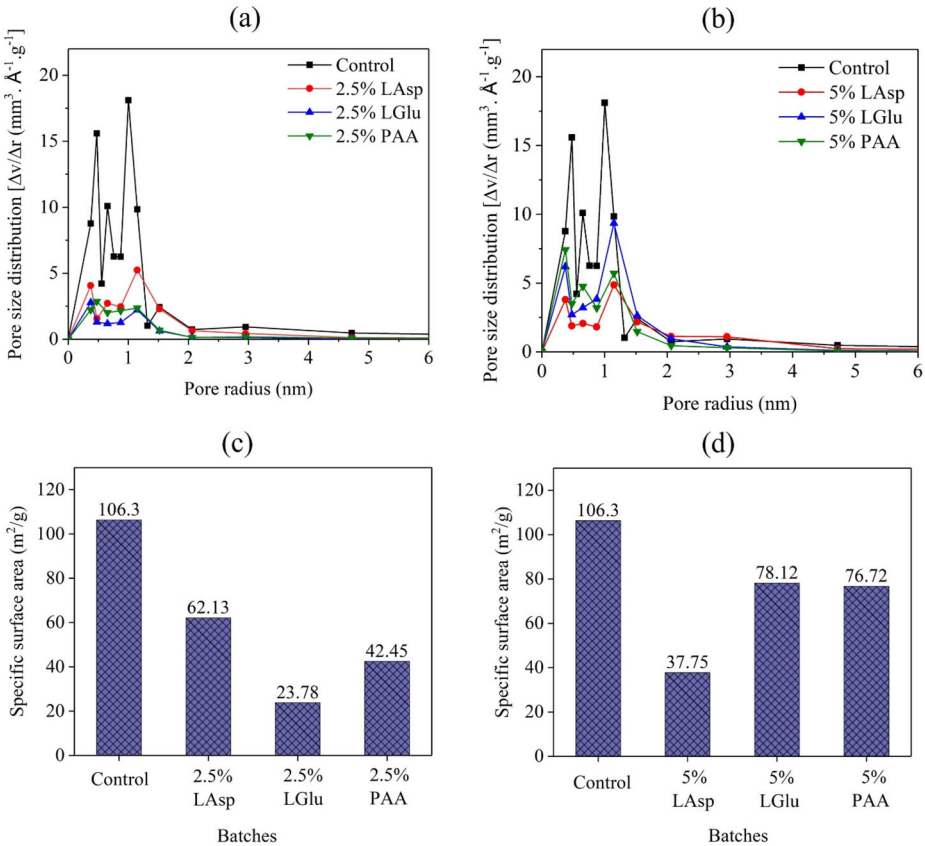

Figure 9. Pore size distribution (a) 2.5% batch and (b) 5% batch; specific surface area (c) 2.5% batch and (d) 5% batch.

the addition of biomimetic molecules decreased the specific surface area of the carbonated matrices compared to the control batch. In a past study [46], it was reported that the formation of metastable carbonates shows a lower surface area compared to the matrix primarily containing calcite. This is because the stabilization of typical metastable carbonates (vaterite and ACC) often occurs due to the coating of the particle by silica gel or the biomimetic molecules. Such a process makes the surface area of the metastable carbonated inaccessible by water molecule and therefore, shows a lower surface area measurement. Accordingly, the reduced surface area in the cases of LGlu and PAA containing batches can be attributed to the formation (and stabilization) of typical metastable carbonates and agglomeration of carbonate particles as observed in the SEM. In the case of LAsp containing batch, the reduced surface area can be attributed to the similar agglomeration of the phases along with reduced degree of carbonation as observed from the TGA.

3.4. *Effects on nanomechanical properties*

Grid nanoindentation technique was applied to each sample over two 60 µm × 60 µm sections, with a total of 200 indentations. Figure 10 shows the elastic modulus (GPa) frequency distribution for the control and biomimetic molecules-modified γ-C_2S paste samples after 7 days of carbonation period. As reported in earlier literature, the elastic moduli of Ca-modified silica gel and $CaCO_3$ found in carbonated cured cementitious composites are approximately 32–42 GPa and 54–79 GPa, respectively [7, 46, 59–61]. Furthermore, the composite phase formed by the mixture of carbonated calcium silicates, consisting of $CaCO_3$ and Ca-modified silica gel, exhibits a mean elastic modulus of approximately 40 GPa [60]. It is worth noting that the elastic modulus of $CaCO_3$ varies significantly due to the formation of different polymorphs. Specifically, the elastic moduli are as follows: 39 GPa for aragonite, 67 GPa for vaterite, and 72 GPa for calcite [62]. The elastic modulus of ACC has not been determined yet. Additionally, distinguishing between vaterite and the composite phase is challenging since they share identical elastic moduli.

From Figure 10(a), it can be observed that the control batch contains tentatively two peaks: one at around 22 GPa, corresponding to HD C-S-H or Ca-modified silica gel and another around 30 GPa, which can be attributed to the carbonate phases with and without mixing with the gel. The batch containing 2.5% LAsp exhibited a distinct peak at approximately 30 GPa in the elastic modulus, suggesting the presence of a single hybrid phase instead of two separate microstructural phases. The mean modulus due to the addition of 2.5% LAsp was increased by 8.5%. In the case of 2.5% LGlu containing batch, two peaks corresponding to the gel and carbonate phases are clearly visible. However, the elastic modulus corresponding to the carbonate phase (~ 40 GPa) was higher in this batch compared to that of the control batch. The mean modulus of the 2.5% LGlu containing batch was 3.5% higher than the control batch. The frequency distribution plot for 2.5% PAA containing batch was similar to that of the 2.5% LAsp batch, as this sample also showed a single peak instead of separate carbonate and gel phases. Therefore, the addition of 2.5% PAA also led to the formation of hybrid phase, i.e. mixture of silica gel and different $CaCO_3$ polymorphs. All of the molecules at 5% dosage showed an increase in the elastic modulus compared to the control batch. Specifically, the highest mean modulus was obtained for the batch containing 5% LGlu batch. This

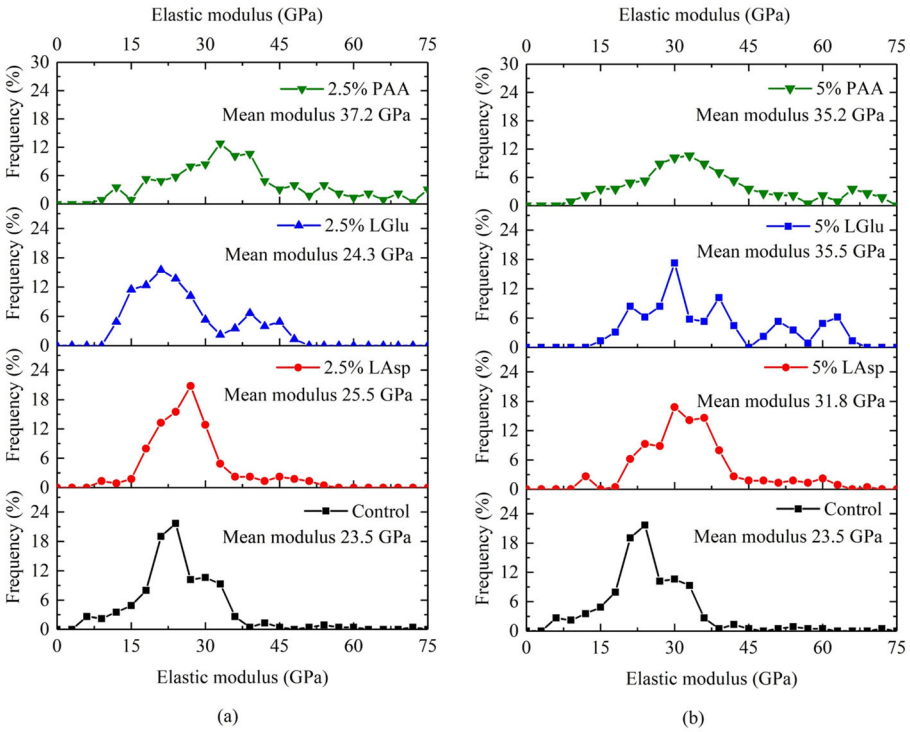

Figure 10. Percent frequency versus elastic modulus (a) 2.5% batches, (b) 5% batches.

study confirms that all of the molecules can effectively enhance the nanomechanical properties of the carbonated γ-C_2S composites.

3.5. Effects on compressive and flexural strengths of ambient temperature cured samples

Figure 11(a) exhibit the compressive strengths of the 7 days carbonated γ-C_2S paste samples with and without the addition of biomimetic molecules. Figure 11(a) shows that 2.5% PAA and 5% LAsp modified γ-C_2S paste samples resulted in 61% and 52% higher strength than the control batch, respectively. Not only these two batches, but all other biomimetic molecules modified batches showed increased compressive strength as well. Under this carbonation condition, PAA was most effective in enhancing the compressive strengths of the carbonated paste samples.

Figure 11(b) shows the flexural strength properties of the 7 days carbonated paste samples. Both 2.5% and 5% dosage increased the flexural strength in the carbonated cementitious system. The flexural strength of the beam samples increased by nearly 54% by the addition of 5% LGlu and 5% LAsp. Even though LAsp modified batch did not show significant $CaCO_3$ polymorphs formation in the microstructure, it enhanced the strength properties because of the adhesion characteristics of aspartic acid [63–65].

3.6. Effects of temperature on strength properties

A separate set of cube and beam samples were cured at elevated temperature (50 °C) to observe the effect of temperature curing on the effectiveness of the biomimetic molecules. It was observed that the elevated temperature enhanced strength gain for both compressive and flexural strengths to a great extent. From Figure 12(a), the results revealed a substantial improvement in strength with increasing temperature. Of particular interest is the effect of different additives, specifically 5% LGlu and 2.5% LGlu, on the strength gain compared to the control batch.

When exposed to elevated temperature curing, 5% LGlu demonstrated the most significant strength enhancement, exhibiting a remarkable 100% increase in strength compared to the control batch. Additionally, 2.5% LGlu exhibited a substantial improvement, with a 69% increase in strength.

Conversely, the LAsp batches did not exhibit any noticeable improvement in strength when subjected to elevated temperature curing. This suggests that the efficacy of LAsp diminishes under high temperature curing conditions. In contrast, the PAA-induced batches displayed a similar percentage increase in compressive strength compared to the batches cured at ambient temperature, indicating that the effects of PAA are consistent regardless of curing temperature.

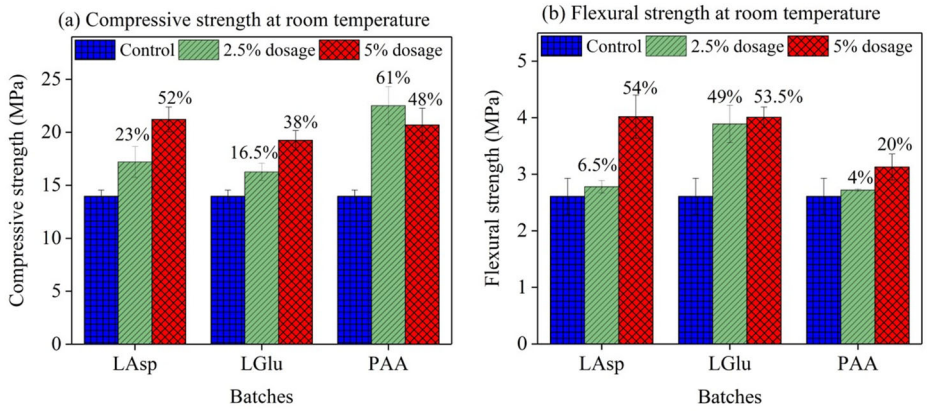

Figure 11. (a) Compressive strength and (b) flexural strength (cured at room temperature and after 7 days of carbonation period).

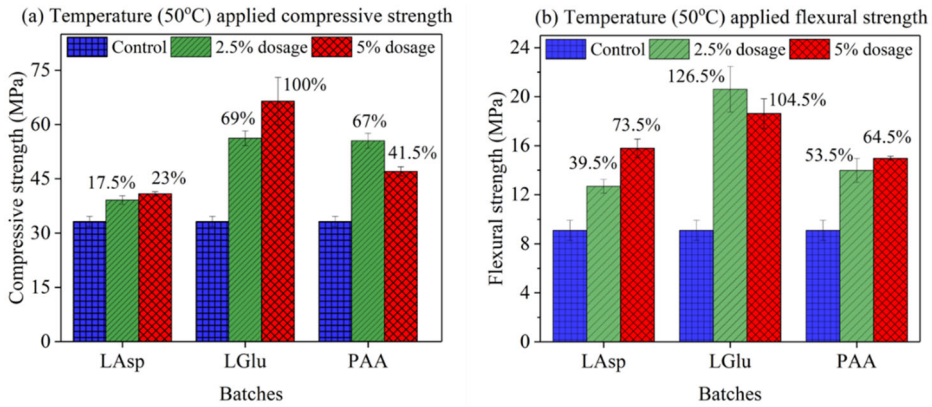

Figure 12. (a) Compressive strength and (b) flexural strength (cured at 50 °C temperature and after 7 days of carbonation period).

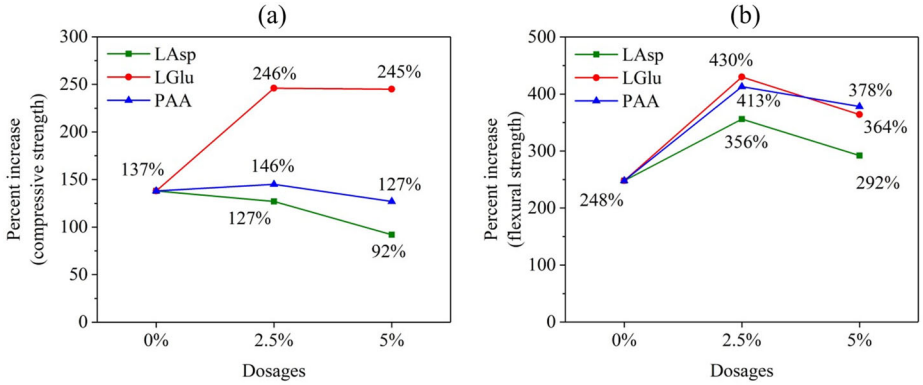

Figure 13. Percent increase of strength after applying temperature curing (a) compressive strength, (b) flexural strength.

The influence of temperature (50 °C) curing on the flexural strength properties of the biomimetic molecules-induced batches is depicted in Figure 12(b). It was evident that the batches subjected to high-temperature curing exhibited improved flexural strength when compared to their counterparts cured at ambient temperature.

Among all the batches, the 2.5% LGlu modified batch demonstrated the most significant increase in flexural strength, registering 126.5% improvement compared to the control batch. Similarly, the 5% LGlu induced batch exhibited a noteworthy increase of 104.5% in flexural strength. Interestingly, the PAA modified batches, in contrast to previous observations, displayed a higher increase in strength when exposed to elevated temperature curing, with increments of 53.5% and 64.5% compared to the control batch. Furthermore, the 5% LAsp modified batch also showed a notable improvement in flexural strength, achieving a 73.5% increase.

These findings underscore the positive impact of high-temperature curing on the flexural strength properties of the biomimetic molecules-induced batches, with specific additives such as LGlu, PAA, and LAsp contributing significantly to these enhancements.

Figure 13 is showcasing the percent increase of the strength compared to the room temperature cured batches. Figure 13(a) shows that, 2.5% LGlu batches improved both compressive strength and flexural strength properties to the maximum. For compressive strength, the percent increase is almost same for the 2.5% and 5% batches. However, for the flexural strength (Figure 13(b)), 2.5% dosage batches enhanced the strength maximum compared to the 5% induced batches.

4. Discussion

This study showed that the selected biomimetic molecules can affect the amounts and polymorphs of the carbonates form in the carbonated γ-C_2S composites. However, effects of these molecules are substantially different due to their different characteristics including surface charge and chain lengths. The observed role of LAsp on carbonated γ-C_2S composites is similar to those observed in the case of carbonated wollastonite [30]. Specifically, with the increasing amounts of LAsp, an increase in the mechanical performance was observed, even though the degree of carbonation was reduced. The negatively charged LAsp forms complex phases with Ca^{2+} surface sites of $CaCO_3$ and subsequently, stabilizes typical metastable polymorphs of $CaCO_3$, including vaterite and ACC, which cause the strength enhancement due to the addition of this molecule [30]. However, due to the same mechanism, LAsp can also form complex with the Ca^{2+} surface sites of γ-C_2S and therefore, reduced the reacting surface area resulting in a reduced degree of carbonation.

While LGlu is also negatively charged as that of LAsp, the effects of LGlu on the carbonated γ-C_2S composites were different. The increased dosage of LGlu enhanced the mechanical performance as well as the degree of carbonation of the composites, and therefore making LGlu a more effective admixture for γ-C_2S compared to the LAsp. Such differences in the roles of LAsp and LGlu are due to their different chain length and solubility (see Figure 14). The solubilities of LGlu and LAsp are 8.6 g/L and 4.5 g/L in water at room temperature. A higher solubility limit is likely to make LGlu more effective in controlling the carbonate polymorphs.

The role of PAA in carbonated composite is different than that of the LGlu and LAsp. Worthy to note, PAA is also negatively charged molecule and a very well-known viscosity modifying admixture for Portland cementitious materials [66,67]. In the case of Portland cement paste, the negatively charged PAA can be adsorbed on the surface of cement particles, which stabilizes the particles in water and therefore, improves the workability of the mixture [66,67]. PAA is also well-known for its ability to alter the $CaCO_3$ crystallization pathway [68,69]. PAA can enable forming $CaCO_3$ with variable crystal shapes, sizes, and polymorphs (vaterite, aragonite, ACC) depending on the dosage, molecular weight, and temperature [68–70]. At 2.5% dosage, PAA increased the compressive strength of the composite by 61% and CO_2 sequestration capacity by nearly 110%. Unlike LAsp and and LGlu, the addition of 2.5% PAA enabled the stabilization of aragonite (observation from FTIR and XRD). Accordingly, the enhanced role of PAA compared to the LAsp and LGlu was attributed to its ability to stabilize aragonite. However, with an increased dosage (5%) of PAA, the strength and CO_2 sequestration capacity were reduced compared to the 2.5% dosage (remained higher than the control and similar to 5% LGlu). This performance reduction at high dosage

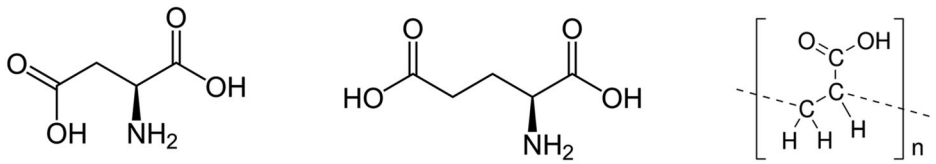

(a) (b) (c)

Figure 14. Molecular structure of (a) L-aspartic acid, (b) L-glutamic acid and (c) polyacrylic acid.

Table 2. Statistical (t-test) analysis results (*p*-values) of compressive and flexural strength at both room and elevated temperatures.

	Strength at room temperature		Strength at 50 °C temperature	
Batches	Compressive strength	Flexural strength	Compressive strength	Flexural strength
2.5% LAsp	0.023	**0.101**	0.003	0.023
5% LAsp	0.001	0.016	0.003	0.011
2.5% LGlu	0.010	**0.069**	8.513E-05	0.020
5% LGlu	0.001	**0.093**	0.005	0.043
2.5% PAA	0.001	**0.093**	0.0002	0.017
5% PAA	0.004	0.020	0.0001	0.017

*Note: Bold fonts represent (*p*-values > 0.05) that the data are not statistically significant.

of PAA was attributed to the excessive adsorption of this molecule on γ-C_2S surface.

Moreover, strength results findings underscore the importance of temperature in the curing process and highlight the varying responses of different additives to elevated temperature conditions. The data demonstrate that LGlu additives can significantly enhance strength under such conditions, while LAsp's effectiveness diminishes, and PAA maintains its consistent performance across curing temperatures. These results offer valuable insights into optimizing the curing process for enhanced material properties.

Table 2 summarizes the p-values from the level of statistical significance. Statistical significance is often quantified by the p-value, represented as p. A small p-value, typically less than or equal to 0.05, indicates strong evidence against the null hypothesis and allows for its rejection. In the analysis, the compressive strength and flexural strength results were compared to those of the control batch, with the test conducted at a 95% confidence level. When p-values below 0.05 were obtained, it indicated a statistically significant difference between the two groups of samples, while p-values exceeding 0.05 suggested the absence of statistical significance between the groups. At room temperature, 5% LAsp and 5% PAA modified batches exhibited statistically significant enhancement in both compressive and flexural strength. When the biomimetic molecules modified batches were cured at 50 °C, all batches containing 2.5% and 5% dosages demonstrated statistical significance in both compressive and flexural strength properties. Among the batches, both the 2.5% and 5% LGlu batches showed significant improvement in strength enhancement at high temperature curing condition.

To sum up, a variety of organic molecules have been used in the past to mimic the biomineralization process of stabilization of $CaCO_3$ polymorphs in carbonation cured calcium silicates [30, 52]. The past evaluated molecules include L-Aspartic, L-Serine, L-Arginine, polydopamine, and cellulose [30, 52]. The application of all of these molecules resulted in improved mechanical performances of the carbonated composites but reduced the CO_2 sequestration in those composites [30, 52]. One of the most interesting observations of the presented study is that both LGlu and PAA were able to enhance the mechanical performance of the composites while also increasing the amounts of CO_2 sequestered in the carbonated γ-C_2S composites.

5. Conclusion

This study's concluding remarks are as follows:

i. The addition of PAA and LGlu increased the amount of $CaCO_3$ formed in the carbonated ɤ-C_2S composites compared to the control batch. Contradictorily, the addition of LAsp reduced the amount of $CaCO_3$ formation.
ii. All the batches showed lower nano-porosity compared to the control batch which resulted in higher compressive strength. Among thebatches carbonated at room temperature, both 5% LAsp and 5% PAA batches showed an increase of compressive strength by nearly 50% . The addition of 2.5% PAA increased the compressive strength by more than 60% for the room temperature carbonated batch.
iii. From nanoindentation results, all the biomimetic molecule containing batches showed higher elastic modulus compared to the control batch.
iv. The addition of 2.5% PAA produced the highest amount of $CaCO_3$ contents and resulted in the

highest compressive strengths after 7 days of carbonation at room temperature.

v. At a curing temperature of 50 °C, both 2.5% and 5% LGlu demonstrated substantial enhancements in both compressive and flexural strengths. Specifically, the addition of 2.5% LGlu resulted in a 69% increase in compressive strength and a remarkable 126.5% improvement in flexural strength. Similarly, the incorporation of 5% LGlu led to a doubling of compressive strength (100%) and a notable increase of 104.5% in flexural strength.

vi. Considering the compressive strengths, the effectiveness of LAsp diminishes during the high temperature carbonation curing and PAA remains nearly equally effective at both of the tested temperatures. However, in terms of flexural strength enhancement, both of these molecules showed a higher effectiveness at 50 °C.

Acknowledgments

Funding for this research was provided by the US National Science Foundation (NSF # ECI -2028462). All opinions, findings, and conclusions or recommendations expressed in this material are those of the authors and do not necessarily reflect the views of the funding agencies.

Disclosure statement

The authors report there are no competing interests to declare.

References

[1] Shi C, Day RL. A calorimetric study of early hydration of alkali-slag cements. Cem Concr Res. 1995;25(6):1333–1346. doi: 10.1016/0008-8846(95)00126-W.

[2] Provis JL, Palomo A, Shi C. Advances in understanding alkali-activated materials. Cem Concr Res. 2015;78:110–125. doi: 10.1016/j.cemconres.2015.04.013.

[3] Chatterjee AK. High belite cements - present status and future technological options: part I. Cem Concr Res. 1996;26(8):1213–1225 doi: 10.1016/0008-8846(96)00099-3.

[4] Quillin K. Performance of belite-sulfoaluminate cements. Cem Concr Res. 2001;31(9):1341–1349 doi: 10.1016/S0008-8846(01)00543-9.

[5] Walling SA, Provis JL. Magnesia-Based cements: a journey of 150 years, and cements for the future? Chem Rev. 2016;116(7):4170–4204. doi: 10.1021/acs.chemrev.5b00463.

[6] De Silva P, Bucea L, Moorehead DR, et al. Carbonate binders: reaction kinetics, strength and microstructure. Cem Concr Compos. 2006;28(7):613–620. doi: 10.1016/j.cemconcomp.2006.03.004.

[7] Ashraf W, Olek J. Carbonation activated binders from pure calcium silicates: reaction kinetics and performance controlling factors. Cem Concr Compos. 2018;93(February):85–98. doi: 10.1016/j.cemconcomp.2018.07.004.

[8] Mrak M, Winnefeld F, Lothenbach B, et al. The influence of calcium sulfate content on the hydration of belite-calcium sulfoaluminate cements with different clinker phase compositions. Mater Struct. 2021;54(212) doi: 10.1617/s11527-021-01811-w.

[9] Ashraf W, Olek J. Carbonation behavior of hydraulic and non-hydraulic calcium silicates: potential of utilizing low-lime calcium silicates in cement-based materials. J Mater Sci. 2016;51(13):6173–6191. doi: 10.1007/s10853-016-9909-4.

[10] Bukowski JM, Berger RL. Reactivity and strength development of CO2 activated non-hydraulic calcium silicates. Cem Concr Res. 1979;9(1):57–68. doi: 10.1016/0008-8846(79)90095-4.

[11] Berger RL, Young JF, Leung K. Acceleration of hydration of calcium silicates by carbon dioxide treatment. Nature Physical Science. 1972;240(97):16–18. doi: 10.1038/physci240016a0.

[12] Goñi S, Guerrero A. Study of alkaline hydrothermal activation of belite cements by thermal analysis. J Therm Anal Calorim. 2010;99(2):471–477. doi: 10.1007/s10973-009-0140-2.

[13] Kubátová D, Zezulová A, Rybová A, et al. Formation of belite-based binder from waste materials. J Therm Anal Calorim. 2020;142(5):1625–1633. doi: 10.1007/s10973-020-10252-6.

[14] Ashraf W. Microstructure of chemically activated of gamma-dicalcium silicate paste. Constr Build Mater. 2018;185:617–627 doi: 10.1016/j.conbuildmat.2018.07.030.

[15] Young JF, Barret P, Bezjak A, et al. Mathematical modelling of hydration of cement: hydration of dicalcium silicate. Mater Struct. 1987;20(5):377–382. doi: 10.1007/BF02472586.

[16] Muhyaddin GF, Asaad DS. Durability aspects of concretes made with boron-activatedhigh belite cement (HBC). Mater Struct. 2022;55(175) doi: 10.1617/s11527-022-02014-7.

[17] Wesselsky A, Jensen OM. Synthesis of pure Portland cement phases. Cem Concr Res. 2009;39(11):973–980. doi: 10.1016/j.cemconres.2009.07.013.

[18] Mu Y, Liu Z, Wang F, et al. Carbonation characteristics of γ-dicalcium silicate for low-carbon building material. Constr Build Mater. 2018;177:322–331. doi: 10.1016/j.conbuildmat.2018.05.087.

[19] Wang YG, Zou BS, Kuo KH, et al. High-resolution electron microscopy study of belite. J Mater Sci. 1989;24(3):877–880. doi: 10.1007/BF01148771.

[20] Chang J, Fang Y, Shang X. The role of β-C2S and γ-C2S in carbon capture and strength development. Mater Struct. 2016;49(10):4417–4424. doi: 10.1617/s11527-016-0797-5.

[21] Higuchi T, Morioka M, Yoshioka I, et al. Development of a new ecological concrete with CO2 emissions below zero. Constr Build Mater. 2014;67(PART C):338–343. doi: 10.1016/j.conbuildmat.2014.01.029.

[22] Yoshioka K, Obata D, Nanjo H, et al. "New ecological concrete that reduces CO2 emissions below zero level ∼ new method for CO2 capture and storage ∼," in. Energy Procedia. 2013;37:6018–6025. doi: 10.1016/j.egypro.2013.06.530.

[23] Saito T, Sakai E, Morioka M, et al. Carbonation reaction of calcium silicate hydrates by hydrothermal synthesis at 150 °C in OPC-γ-Ca2SiO4-α-quartz systems. ACT. 2007;5(3):333–341. doi: 10.3151/jact.5.333.

[24] Jiang T, Cui K, Chang J. Development of low-carbon cement: carbonation of compounded C2S by β-C2S and γ-C2S. Cem Concr Compos. 2023;139:105071. doi: 10.1016/j.cemconcomp.2023.105071.

[25] Chang J, Jiang T, Cui K. Influence on compressive strength and CO2 capture after accelerated carbonation of combination β-C2S with γ-C2S. Constr Build Mater. 2021;312:125359. doi: 10.1016/j.conbuildmat.2021.125359.

[26] Fang Y, Chang J. Rapid hardening β-C2S mineral and microstructure changes activated by accelerated carbonation curing. J Therm Anal Calorim. 2017;129(2):681–689. doi: 10.1007/s10973-017-6165-z.
[27] Guan X, Liu S, Feng C, et al. The hardening behavior of γ-C2S binder using accelerated carbonation. Constr Build Mater. 2016;114:204–207. doi: 10.1016/j.conbuildmat.2016.03.208.
[28] Bernal SA, Provis JL, Walkley B, et al. Gel nanostructure in alkali-activated binders based on slag and fly ash, and effects of accelerated carbonation. Cem Concr Res. 2013;53:127–144. doi: 10.1016/j.cemconres.2013.06.007.
[29] Moorehead DR. Cementation by the carbonation of hydrated lime. Cem Concr Res. 1986;16(5):700–708. doi: 10.1016/0008-8846(86)90044-X.
[30] Khan RI, Ashraf W, Olek J. Amino acids as performance-controlling additives in carbonation-activated cementitious materials. Cem Concr Res. 2021;147:106501. doi: 10.1016/j.cemconres.2021.106501.
[31] Lu B, Drissi S, Liu J, et al. Effect of temperature on CO2 curing, compressive strength and microstructure of cement paste. Cem Concr Res. 2022;157:106827. doi: 10.1016/j.cemconres.2022.106827.
[32] Shi C, Qu B, Provis JL. Recent progress in low-carbon binders. Cem Concr Res. 2019;122(April):227–250. doi: 10.1016/j.cemconres.2019.05.009.
[33] Baffoe E, Ghahremaninezhad A. Effect of proteins on the mineralization, microstructure and mechanical properties of carbonation cured calcium silicate. Cem Concr Compos. 2023;141:105121. Aug. doi: 10.1016/j.cemconcomp.2023.105121.
[34] Wu F, You X, Wang M, et al. Increasing flexural strength of CO2 cured cement paste by CaCO3 polymorph control. Cem Concr Compos. 2023;141:105128. Aug. doi: 10.1016/j.cemconcomp.2023.105128.
[35] Nawarathna THK, Nakashima K, Kawabe T, et al. Artificial fusion protein to facilitate calcium carbonate mineralization on insoluble polysaccharide for efficient biocementation. ACS Sustainable Chem. Eng. 2021;9(34):11493–11502. doi: 10.1021/acssuschemeng.1c03730.
[36] Polowczyk I, Bastrzyk A, Fiedot M. Protein-mediated precipitation of calcium carbonate. Materials. 2016;9(11):944. doi: 10.3390/ma9110944.
[37] Yang H, Yao W, Yang L, et al. The self-assembly of CaCO3 crystals in the presence of protein. J Cryst Growth. 2009;311(9):2682–2688. doi: 10.1016/j.jcrysgro.2009.02.049.
[38] Kim Y-Y, Carloni JD, Demarchi B, et al. Tuning hardness in calcite by incorporation of amino acids. Nat Mater. 2016;15(8):903–910. doi: 10.1038/nmat4631.
[39] Kim HL, Shin YS, Yang SH. Effect of poly(acrylic acid) on crystallization of calcium carbonate in a hydrogel. CrystEngComm. 2022;24(7):1344–1351. doi: 10.1039/D1CE01687C.
[40] Goto S, Suenaga K, Kado T, et al. Calcium silicate carbonation products. J Amer Ceram Soc. 1995;78(11):2867–2872. doi: 10.1111/j.1151-2916.1995.tb09057.x.
[41] Berliner R, Ball C, West PB. Neutron powder diffraction investigation of model cement compounds. Cem Concr Res. 1997;27(4):551–575. doi: 10.1016/S0008-8846(97)00028-8.
[42] Sáez Del Bosque IF, Martínez-Ramírez S, Blanco-Varela MT. FTIR study of the effect of temperature and nanosilica on the nano structure of C-S-H gel formed by hydrating tricalcium silicate. Constr Build Mater. 2014;52:2049–2056 doi: 10.1016/j.conbuildmat.2013.10.056.
[43] Odler I. The BET-specific surface area of hydrated Portland cement and related materials. Cem Concr Res. 2003;33(12):2049–2056. doi: 10.1016/S0008-8846(03)00225-4.
[44] Brunauer S, Emmett PH, Teller E. Adsorption of gases in multimolecular layers. J. Am. Chem. Soc. 1938;60(2):309–319. doi: 10.1021/ja01269a023.
[45] Barrett EP, Joyner LG, Halenda PP. The determination of pore volume and area distributions in porous substances. I. Computations from nitrogen isotherms. J. Am. Chem. Soc. 1951;73(1):373–380. doi: 10.1021/ja01145a126.
[46] Ashraf W, Olek J. Elucidating the accelerated carbonation products of calcium silicates using multi-technique approach. J CO2 Util. 2018;23:61–74. doi: 10.1016/j.jcou.2017.11.003.
[47] Panesar DK, Francis J. Influence of limestone and slag on the pore structure of cement paste based on mercury intrusion porosimetry and water vapour sorption measurements. Constr Build Mater. 2014;52:52–58. doi: 10.1016/j.conbuildmat.2013.11.022.
[48] Ashraf W, Olek J, Tian N. Multiscale characterization of carbonated wollastonite paste and application of homogenization schemes to predict its effective elastic modulus. Cem Concr Compos. 2016;72:284–298. doi: 10.1016/j.cemconcomp.2016.05.023.
[49] Khan RI, Siddique S, Ashraf W. Effects of magnesia in semi-hydraulic and non-hydraulic calcium silicate binders during carbonation curing. Constr Build Mater. 2022;338:127628. Jul. doi: 10.1016/j.conbuildmat.2022.127628.
[50] Lee, Sung-Hyun, Kim, Kyungnam, Song, Myong-Shin, Mabudo, "Physical and chemical properties of cement mortar with gamma-C2S,"J. Korean Ceram. Soc, vol. 53, no. 2, 194, 199, 2016, doi: 10.4191/kcers.2016.53.2.194.
[51] Sow PY. IR - Spectroscopic investigations of the kinetics of calcium carbonate precipitation University Konstanz, 2016.
[52] Khan RI, Haque MI, Ashraf W, et al. Role of biopolymers in enhancing multiscale characteristics of carbonation-cured cementitious composites. Cem Concr Compos. 2022;134:104766. doi: 10.1016/j.cemconcomp.2022.104766.
[53] Andersen FA, Brečević L, Beuter G, et al. Infrared spectra of amorphous and crystalline calcium carbonate. Acta Chem. Scand. 1991;45:1018–1024. doi: 10.3891/acta.chem.scand.45-1018.
[54] Weir CE, Lippincott ER. Infrared studies of aragonite, calcite, and vaterite type structures in the borates, carbonates, and nitrates. J Res Natl Bur Stand A Phys Chem. 1961;65A(3):173–180. doi: 10.6028/jres.065a.021.
[55] Sato M, Matsuda S. Structure of vaterite and infrared spectra. Zeitschrift Fur Kristallographie - New Crystal Structures. 1969;129(5-6):405–410. doi: 10.1524/zkri.1969.129.5-6.405.
[56] Chakrabarty D, Mahapatra S. Aragonite crystals with unconventional morphologies. J. Mater. Chem. 1999;9(11):2953–2957. doi: 10.1039/a905407c.
[57] Zhou GT, Yu JC, Wang XC, et al. Sonochemical synthesis of aragonite-type calcium carbonate with different morphologies. New J. Chem. 2004;28(8):1027. doi: 10.1039/b315198k.
[58] Baroghel-Bouny V. Water vapour sorption experiments on hardened cementitious materials. Cem Concr Res. 2007;37(3):414–437. doi: 10.1016/j.cemconres.2006.11.019.
[59] Constantinides G, Ravi Chandran KS, Ulm FJ, et al. Grid indentation analysis of composite microstructure and mechanics: principles and validation. Mater Sci Eng, A. 2006;430(1–2):189–202. doi: 10.1016/j.msea.2006.05.125.
[60] Ashraf W, Olek J, Jain J. Microscopic features of non-hydraulic calcium silicate cement paste and mortar. Cem Concr Res. 2017;100:361–372. doi: 10.1016/j.cemconres.2017.07.001.

[61] Miller M, Bobko C, Vandamme M, et al. Surface roughness criteria for cement paste nanoindentation. Cem Concr Res. 2008;38(4):467–476. doi: 10.1016/j.cemconres.2007.11.014.
[62] Dhami NK, Mukherjee A, Reddy MS. Micrographical, minerological and nano-mechanical characterisation of microbial carbonates from urease and carbonic anhydrase producing bacteria. Ecol Eng. 2016;94:443–454. Sep. doi: 10.1016/j.ecoleng.2016.06.013.
[63] Willett RL, Baldwin KW, West KW, et al. Differential adhesion of amino acids to inorganic surfaces. Proc Natl Acad Sci U S A. 2005;102(22):7817–7822. doi: 10.1073/pnas.0408565102.
[64] Schussler O, Coirault C, Louis-Tisserand M, et al. Use of arginine-glycine-aspartic acid adhesion peptides coupled with a new collagen scaffold to engineer a myocardium-like tissue graft. Nat Clin Pract Cardiovasc Med. 2009;6(3):240–249. doi: 10.1038/ncpcardio1451.
[65] Hwang JJ, Stupp SI. Poly(amino acid) bioadhesives for tissue repair. J Biomater Sci Polym Ed. 2000;11(10):1023–1038. doi: 10.1163/156856200743553.
[66] Ma B, Peng Y, Tan H, et al. Effect of polyacrylic acid on rheology of cement paste plasticized by polycarboxylate superplasticizer. Materials. 2018;11(7):1081. Jun. doi: 10.3390/ma11071081.
[67] Guo Y, Ma B, Zhi Z, et al. Effect of polyacrylic acid emulsion on fluidity of cement paste. Colloids Surf A Physicochem Eng Asp. 2017;535:139–148. Dec. doi: 10.1016/j.colsurfa.2017.09.039.
[68] Ouhenia S, Chateigner D, Belkhir MA, et al. Synthesis of calcium carbonate polymorphs in the presence of polyacrylic acid. J Cryst Growth. May 2008;310(11):2832–2841. doi: 10.1016/j.jcrysgro.2008.02.006.
[69] Watamura H, Sonobe Y, Hirasawa I. Polyacrylic acid-Assisted crystallization phenomena of carbonate crystals. Chem Eng & Technol. 2014;37(8):1422–1426. doi: 10.1002/ceat.201400017.
[70] Huang SC, Naka K, Chujo Y. Effect of molecular weights of poly(acrylic acid) on crystallization of calcium carbonate by the delayed addition method. Polym J. 2008;40(2):154–162. doi: 10.1295/polymj.PJ2007162.